

Orbital magnetic moments in pure and doped carbon nanotubes

Magdalena Margańska*, Marek Szopa, Elżbieta Zipper

Department of Theoretical Physics, University of Silesia, ul Uniwersytecka 4, 40 007 Katowice, Poland

The unusual band structure of carbon nanotubes (CNs) results in their remarkable magnetic properties. The application of magnetic field parallel to the tube axis can change the conducting properties of the CN from metallic to semiconducting and vice versa. Apart from that \mathbf{B} induces (via the Bohm-Aharonov effect) orbital magnetic moments μ_{orb} in the nanotube. These moments are studied both in pure and hole- or electron-doped CNs, isolated or in a circuit. Remarkably, μ_{orb} in pure CNs depends uniquely on their original conducting properties, length, and temperature but it does not depend on the nanotube radius or the particular chirality. In doped nanotubes the magnetic moments can be strongly altered and depend on the radius and chirality. Temperature can even change their character from diamagnetic at low T to paramagnetic at high T . A full electron-hole symmetry in doped tubes is also revealed.

PACS numbers: 75.75.+a, 73.22.-f, 73.23.Ra

I. INTRODUCTION

The electronic fate of a carbon nanotube (CN) is in general determined once it has been grown. Depending on the radius and the chiral angle it can be semiconducting or metallic. The electronic properties of CN can however be modulated by coaxial magnetic field via the Bohm-Aharonov (BA) effect which can turn a metallic CN into a semiconducting one and vice versa. This has been predicted by Ajiki and Ando [1] and observed recently in three independent measurements [2, 3, 4]. CN have an ideal structure for studying the effect of the BA flux on the energy spectrum. A magnetic field \mathbf{B} introduces a phase factor in the electron wave function in the circumferential direction and leads to a shift in the energy bands. The value of the energy shift depends on the strength of the applied field and on the orbital magnetic moment. This can be observed e.g. as a change in the band gap structure by measuring the conductance of a single nanotube suspended between two electrodes [2, 3]. The magnetic field influences the motion of electrons around the circumference of CN, giving rise to persistent currents [5, 6] which at low temperatures do not decay. Persistent current multiplied by the CN cross section give the orbital magnetic moment μ_{orb} directed along the axis.

In the present paper we calculate μ_{orb} in single-wall CNs in the tight binding approximation for various chiralities, lengths and radii (provided that $R > 10\text{\AA}$), for a range of electron or hole doping values. We study both isolated nanotubes, where the number of electrons $N_e = \text{const}$ and nanotubes connected to a particle reservoir (e.g. as a part of a circuit), where the chemical potential $\mu_{chem} = \text{const}$.

We find that in undoped nanotubes the character of the magnetic moment depends only on the CN's conducting properties (i.e. whether the tube is metallic or semicon-

ducting), its length and the temperature of the system. On the other hand, in hole- or electron doped nanotubes the behaviour of $\mu_{orb}(\phi)$ depends strongly on the chirality of the nanotube, on its size, and on the degree of hole or electron doping.

In our model calculations we study nanotubes in the ballistic regime and we work in the non-interacting electrons approximation which has yielded good agreement with experimental results in mesoscopic rings [7] and in carbon nanotubes [3, 8, 9].

II. THE MODEL

Carbon nanotubes are commonly considered and analysed as rolled-up graphene planes. We follow here the same approach, working in the basis in which the lattice generators are $\mathbf{T}_1 = \sqrt{3}e_x$, $\mathbf{T}_2 = \sqrt{3}/2e_x + 3/2e_y$, and the length unit is the length of the $C - C$ bond, 1.42\AA [10, 11]. A nanotube is uniquely defined by four parameters $(m_1, m_2) \times (p_1, p_2)$, which define its circumference and length vectors:

$$\begin{aligned} \mathbf{L}_\perp &= m_1\mathbf{T}_1 + m_2\mathbf{T}_2 & \text{for the circumference,} \\ \mathbf{L}_\parallel &= p_1\mathbf{T}_1 + p_2\mathbf{T}_2 & \text{for the length.} \end{aligned} \quad (1)$$

In most theoretical works on carbon nanotubes the tube under examination is considered to be infinitely long, resulting in a continuous spectrum of momenta along the CN. Since the real CNs are very long but finite, we consider $L_\parallel < \infty$. Therefore, the momentum is quantized in both directions. We chose the longitudinal boundary conditions to be cyclic:

$$\mathbf{k} \cdot \mathbf{L}_\parallel = 2\pi l_\parallel, \quad l_\parallel \in \mathbb{Z}, \quad (2)$$

where \parallel stands for the direction parallel to the length of the nanotube. We found no significant differences between currents in cyclic and open longitudinal boundary conditions (see also [12]).

The magnetic field is applied parallel to the axis of

*corresponding author: magda@phys.us.edu.pl

the CN. The Aharonov-Bohm phase factor modifies the transverse boundary condition (in the direction perpendicular to the magnetic field):

$$\mathbf{k} \cdot \mathbf{L}_\perp = 2\pi(l_\perp + \frac{\phi}{\phi_0}), \quad l_\perp \in \mathbb{Z}, \quad (3)$$

where \perp stands for the direction parallel to the circumference of the nanotube, ϕ is the magnetic flux and $\phi_0 = h/e$ is the quantum flux unit. The momentum vector \mathbf{k} can be defined either in the (k_x, k_y) or (k_\perp, k_\parallel) basis. We use the second one throughout our calculations, the first only in the dispersion relation. When $\phi \neq 0$, the currents carried by states with \mathbf{k} and $-\mathbf{k}$ do not cancel out, and a net current appears. At fields accessible in labs only a part of the Bohm-Aharonov period ϕ_0 could be observed in nanotubes of small diameter. For example, in a CN with radius $R = 25\text{\AA}$ a magnetic field B of the order of 210T is required to observe the full ϕ_0 period.

Currents running along the circumference of the CN induce in the nanotube a magnetic moment parallel to its axis. The magnetic moment of an electron close to the Fermi level can also be calculated by the following reasoning.

The energy gap between conduction and valence states close to the Fermi surface (FS) is

$$E_g^0 = \hbar v_F(k_\perp - K_i), \quad i = 1, 2, \quad (4)$$

where K_i are the Fermi points where the valence and conduction bands of graphene meet. The Bohm-Aharonov effect shifts the allowed k_\perp by $\delta k_\perp(\phi)$,

$$k_\perp(\phi) = k_\perp + \delta k_\perp(\phi), \quad \delta k_\perp(\phi) = \frac{\phi}{R\phi_0}, \quad (5)$$

resulting also in the energy shift ΔE [2],

$$\Delta E \simeq \frac{\partial E}{\partial k_\perp} \big|_{k_F} \delta k_\perp(\phi) = \pm \frac{\hbar v_F}{R} \frac{\phi}{\phi_0} = \vec{\mu}_{orb}^F \cdot \mathbf{B}, \quad (6)$$

where $\vec{\mu}_{orb}^F$ is the orbital magnetic moment of an electron at (or the closest to) the Fermi surface

$$\vec{\mu}_{orb}^F = \frac{Re v_F}{2} \mathbf{e}_\parallel \quad (7)$$

(\mathbf{e}_\parallel is the unit vector along the CN axis). This shift of the energy states results in the change of the band gap and can convert a metallic CN into a semiconducting one and vice versa. Therefore, from now on by 'metallic' and 'semiconducting' we understand CN's which display this behaviour at $\phi = 0$.

The change of the band gap with the magnetic field has been investigated in three independent measurements [2, 3, 4] and in the first one helped to determine the magnitude of the orbital magnetic moment of an electron at the FS, μ_{orb}^F . A good agreement between the experimental and the theoretical values has been found [2]. Nevertheless, the magnetic response of a CN is determined by its full magnetic moment, given by

$$\mu_{orb}(\phi, T) = -\pi R^2 \frac{\partial F(\phi, T)}{\partial \phi}, \quad (8)$$

where $F(\phi, T)$ is the free energy of the CN. In other words, μ_{orb} can be written in terms of the total current $I(\phi, T)$, which runs at the cylindrical surface in the presence of the magnetic field (for detailed derivation see [13]).

$$\begin{aligned} \mu_{orb}(\phi, T) &= \pi R^2 I(\phi, T) = \\ &= \pi R^2 \sum_{k_\perp, k_\parallel} \frac{1}{1 + \exp[(E_{\mathbf{k}}(\phi) - \mu_{chem}(\phi))/kT]} I_{\mathbf{k}}(\phi). \end{aligned} \quad (9)$$

The sum runs over the whole Brillouin zone (BZ). This current is persistent at low T . In our paper we investigate the dependence of $\mu_{orb}(\phi, T)$ on temperature, nanotube parameters (radius, chirality, length) and the value of the chemical potential which changes with doping. This is an extension of the work of Ajiki and Ando [1], who calculated the magnetic moment μ_{orb} for an undoped tube at $T = 0$.

The currents carried by individual momentum states at $T = 0$ are

$$I_{\mathbf{k}}(\phi) = -\frac{\partial E_{\mathbf{k}}}{\partial \phi} = -\frac{\partial E_{\mathbf{k}}}{\partial k_\perp} \frac{\partial k_\perp}{\partial \phi} = -\frac{\partial E_{\mathbf{k}}}{\partial k_\perp} \frac{2\pi}{\phi_0 |\mathbf{L}_\perp|}, \quad (10)$$

where the form of $E(\mathbf{k})$ depends on the approximation used. Our choice is the tight binding approximation, commonly used in calculations involving graphene structures. Consequently, the dispersion relation is [10, 11]

$$E_{\mathbf{k}} = \pm \gamma \sqrt{1 + 4 \cos^2(\frac{\sqrt{3}}{2} k_x) + 4 \cos(\frac{\sqrt{3}}{2} k_x) \cos(\frac{3}{2} k_y)}, \quad (11)$$

where γ is the hopping integral for graphene. Various authors assume different values for γ , ranging from 2.5 eV to 3 eV [3, 14].

The individual currents $I_{\mathbf{k}}(\phi)$ in Eq. (10) depend on the position of the \mathbf{k} states in the Brillouin zone. The level of μ_{chem} defines the Fermi surface and determines the range of states whose contributions dominate the sum (9). The distribution of allowed momentum states in the BZ depends on the chirality of the CN. Therefore at shifted μ_{chem} different states fall into the dominating range depending on the chirality of the nanotube. Consequently the total magnetic moment depends on the doping level and on the chirality of the CN.

At the half-filling, corresponding to undoped nanotube, the chemical potential is 0 ($\mu_{chem} = 0$). Doped systems (either doped with electrons or with holes) can be studied under two different physical conditions.

If the system is connected with a particle reservoir, its chemical potential at a given doping is constant ($\mu_{chem} = \text{const}$). The distribution of allowed momentum states in the BZ shifts with the magnetic flux which induces a shift of the Fermi level. But the chemical potential is determined externally and the CN can absorb the number of electrons or holes necessary to keep it stable. The number of electrons then changes with the magnetic flux, $N_e = N_e(\phi)$.

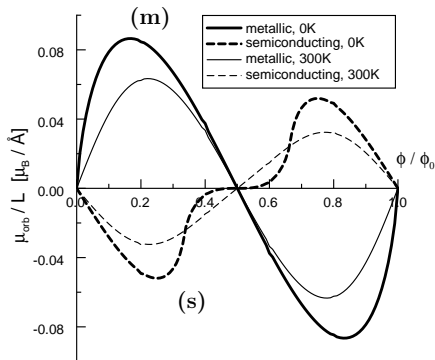


FIG. 1: Orbital magnetic moment per \AA in a single-wall nanotube of radius 25\AA , for different chiralities. All metallic nanotubes have the same (up to 1%) $\mu_{orb}(\phi)$. The same is true for the semiconducting nanotubes. Thick lines are orbital magnetic moments at $T = 0\text{K}$, thin lines – at $T = 300\text{K}$.

When the nanotube is isolated, there is no exchange of electrons with a reservoir, their number is constant ($N_e = \text{const}$) and the chemical potential is a function of the magnetic flux ($\mu_{chem} = \mu_{chem}(\phi)$). The magnetic moments have in general different shape in isolated than in connected nanotubes. We performed the calculations in both cases.

We have calculated numerically the magnetic moment according to Eq. (9). In the case of constant number of electrons the chemical potential has been found at each value of ϕ from the condition $\sum_{(k_\perp, k_\parallel)} f_{FD}(E_{(k_\perp, k_\parallel)}(\phi)) = N_e$, where $f_{FD}(E_{\mathbf{k}}(\phi))$ is the Fermi-Dirac distribution function.

III. ORBITAL MAGNETIC MOMENTS – UNDOPED NANOTUBES

Several effects concerning the persistent currents and induced magnetic moments in parallel magnetic field can be deduced from an analysis of the structure of the energy spectrum and the Brillouin zone. In this Section we discuss undoped nanotubes i.e. $\mu_{chem} = 0$. In this case there is no difference between the $\mu_{chem} = \text{const}$ and $N_e = \text{const}$ conditions. The number of states below the Fermi level is the same as in the Brillouin zone, consequently, $N_e = \text{const}$ regardless of the value of the external magnetic flux. The energy gap opens or closes with changing ϕ , but the chemical potential is fixed at 0.

$\mu_{orb}(\phi, T)$ in metallic and semiconducting CN's. There are two types of behaviour of $\mu_{orb}(\phi, T)$. In metallic nanotubes it is paramagnetic at $\phi = 0$, in semiconducting ones it is diamagnetic. This effect does not depend on the particular chirality of the metallic or semiconducting nanotube. It is so because the main component of the magnetic moment (9) comes from the

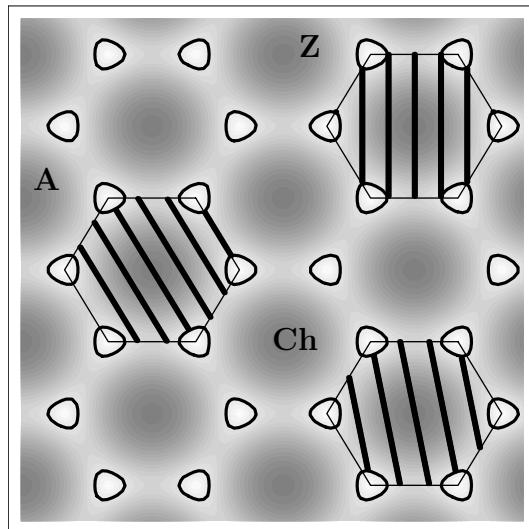


FIG. 2: The reciprocal lattice of graphene, with momentum states and first Brillouin zones of **Zigzag** (5,0), **Armchair** (3,3), and **Chiral** (4,1) nanotubes doped to -0.6γ . The Fermi contours are the thick triangular loops and the thick straight lines correspond to $k_\perp = \text{const}$ lines. In undoped nanotubes all momentum states in the Brillouin zone enter into the sum from Eq. (9) and $\mu_{orb}(\phi)$ is chirality-independent. In doped nanotubes only those states which lie below the Fermi level (outside the loops) contribute to the sum. Note that the number of missing states (the missing fragments of $k_\perp = \text{const}$ lines) is different in **A**, **Z** and **Ch** cases, which results in the chirality dependence of $\mu_{orb}(\phi)$.

\mathbf{k} states close to the Fermi points \mathbf{K}_i . The dispersion relation in the neighbourhood of these points has a form of two cones and therefore rotational symmetry [15]. Because of that $\partial E/\partial k_\perp$ is independent of the particular angle (determined by m_1 and m_2) at which $k_\perp = \text{const}$ lines (see Fig. 2) lie with respect to the edges of the Brillouin zone. In the case of metallic CNs these momentum lines cross the Fermi points (see Fig 5a) and the magnetic moment has the (m) shape from Fig. 1. Due to the peculiar band structure of the CNs, the magnetic moment in a semiconducting CN (s) has an unusual shape, with a plateau around $\phi_0/2$. Close inspection of the structure of momentum lines in the BZ shows that it is a superposition of two metallic moments, shifted by $\pm\phi_0/3$ (it is shown in Fig. 3). They are generated by the two momentum ($k_\perp = \text{const}$) lines which reach the Fermi point, one at $\phi = \phi_0/3$, the other at $2\phi_0/3$, independently of chirality. The amplitude of this sum is then smaller than in the metallic CN, where both momentum lines reach the Fermi points at the same ϕ . The slope of μ_{orb} vs. ϕ (see Fig 1) is steeper for these values of ϕ where the CN is metallic, since the paramagnetic behaviour of the μ_{orb} is caused by momentum states crossing the Fermi surface, whose contributions to the magnetic moment are the most significant. On the contrary, the gentle

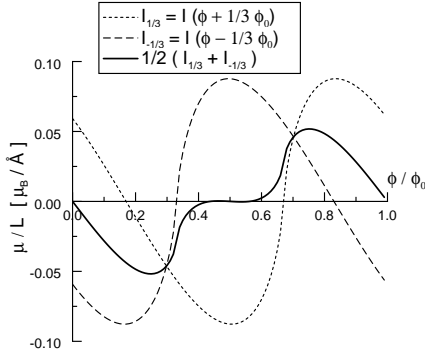


FIG. 3: The magnetic moment per \AA in a semiconducting nanotube as a superposition of two metallic moments shifted by $\pm\phi_0/3$.

slope of μ_{orb} in the semiconducting regime is caused by the diamagnetism of the states below the FS.

Temperature dependence. The magnitude of the orbital magnetic moment, contrary to the spin magnetic moment, decreases with temperature although this decrease is not very dramatic for the ranges of magnetic field accessible in labs. It is more important for CN with larger R , i.e. for multiwall CN, and the measurements should then be performed at lower T . Since the main effect of temperature on $\mu_{orb}(\phi, T)$ on undoped nanotubes is a suppression of its amplitude (cf. Fig. 1), we shall in this Section assume $T = 0$ and analyse only $\mu_{orb}(\phi, 0)$ which we shall denote by $\mu_{orb}(\phi)$.

When the distance between momentum lines Δk_\perp becomes small enough (i.e. when $R > 10\text{\AA}$), $I_k(\phi, T)$ is linear in Δk_\perp and two effects appear.

Length-scaling of the magnetic orbital moments. The sum of $I(\mathbf{k})$ grows linearly with the number of states on one momentum ($k_\perp = \text{const}$) line, which is proportional to the length of the nanotube. This is also true for doped nanotubes.

Independence of $\mu_{orb}(\phi)$ of the nanotube radius.

The radius of the nanotube affects $\mu_{orb}(\phi)$ in two ways.

- 1) The cross section of a nanotube $\sim R^2$.
- 2) From Eq. (10) we conclude that the current of an individual \mathbf{k} state $\sim 1/R$ because $\partial E_{\mathbf{k}}/\partial k_\perp$ is constant for a given \mathbf{k} . The summation over the whole Brillouin zone in Eq. (9) yields another $1/R$ factor and as a result the whole sum is proportional to $1/R^2$.

These two effects lead to $\mu_{orb}(\phi)$ nearly independent of R (see black circles in Fig. 4), in agreement with [1]. This result in undoped CN's does not depend on the chirality of the nanotube. Note that $\mu_{orb}^F(\phi)$ calculated and measured in [2] increases linearly with R because it is due only to electrons closest to the Fermi level.

Thus for any undoped metallic or semiconducting nanotube the total magnetic moment depends only on its length and on temperature, and has either the (m) (in

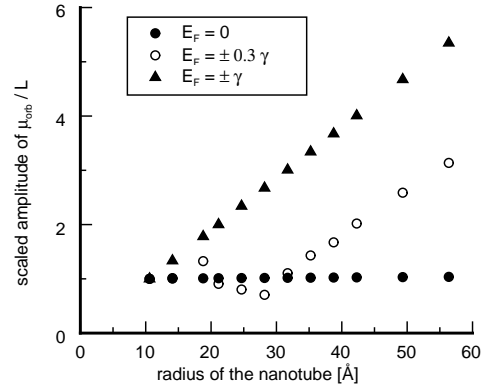


FIG. 4: The dependence of the magnetic moment per unit length on the nanotube radius in zigzag nanotubes ranging from (27,0) to (144,0), at half-filling and at two values of doping. The amplitude of the μ_{orb} on the vertical axis is scaled with respect to the values obtained for the first nanotube, with $R = 10.59\text{\AA}$.

metallic CN's) or the (s) (in semiconducting CN's) form from Fig. 1.

IV. ORBITAL MAGNETIC MOMENTS – DOPED NANOTUBES

The peculiar band structure of graphene is reflected in the variety of behaviours of CNs with different chiralities upon doping. We performed the calculations of the full magnetic moment $\mu_{orb}(\phi, T)$ for zigzag, armchair and chiral nanotubes. We found that it depends significantly on doping; being the sum of the terms below the FS it depends strongly on the shape of the FS which changes with the number of holes or electrons introduced in the system.

Isolated or connected: $\mu_{chem} = \text{const}$ versus $N_e = \text{const}$ approach. Different results were obtained for $\mu_{chem} = \text{const}$ (nanotube in a circuit) and $N_e = \text{const}$ (isolated nanotube). Both conditions can be realized experimentally. The calculations were performed for both electron and hole doping, changing the Fermi level from $E_F = 0$ (no doping) to $E_F = \pm\gamma$. In the case of nanotubes doped to $E_F = \pm\gamma$ we found that again there is no difference between $N_e = \text{const}$ and $\mu_{chem} = \text{const}$, because the Fermi contour has then the hexagonal symmetry of the Brillouin zone (cf. Fig. 5d) and the number of momentum states within it is constant with ϕ . At intermediate doping the two approaches give distinctly different results which are shown in Fig. 6.

Dependence of $\mu_{orb}(\phi)$ on the nanotube radius. The independence of $\mu(\phi, T)$ on the radius of the nanotube shown in Fig. 4 is characteristic for undoped nanotubes only. The sum in Eq. (9) is in that case over the whole Brillouin zone and the dominating currents come

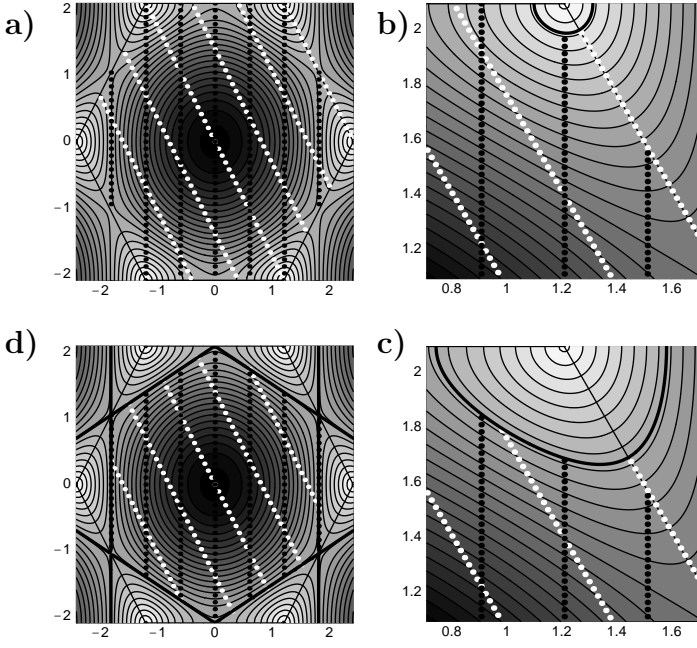


FIG. 5: The Brillouin zone and momentum states of an arbitrary armchair (white dots) and zigzag (black dots) nanotube of similar radius, at $\phi = 0$. The background is the contour plot of $E_{\mathbf{k}}$ from Eq. (11). The Fermi contour is marked by thick solid lines. a) Full Brillouin zone, undoped nanotube ($\mu_{chem} = 0$). The Fermi surface reduces to two points at the vertices of the hexagon. b) The neighbourhood of the Fermi point $(2\pi/(3\sqrt{3}), 2\pi/3)$, $\mu_{chem} = -0.16\gamma$. The contour is circular and both nanotubes respond with almost the same magnetic moments (see Fig. 10), momentum lines cross the Fermi contour at identical angles. c) The neighbourhood of the Fermi point $(2\pi/(3\sqrt{3}), 2\pi/3)$, $\mu_{chem} = -0.6\gamma$. The Fermi contour loses the rotational symmetry and magnetic moments in zigzag and armchair nanotubes differ (see Fig. 11). d) Full Brillouin zone, $\mu_{chem} = -\gamma$. The Fermi contour is a closed hexagon, with two sides parallel to the momentum lines in the zigzag nanotube. Currents in this tube are very strongly enhanced, in others nearly vanishing.

from the momentum states in the neighbourhood of the Fermi points \mathbf{K}_i , where the dispersion relation is conical. On the other hand, if the doping is to $E_F = \pm\gamma$, the amplitude of $\mu_{orb}(\phi, T)$ grows linearly with the radius of the nanotube (for illustration in zigzag case, see Fig. 4). The currents dominating the sum are those from the states near the Fermi contour which in this case is the inner hexagone in Fig. 5d; the dispersion relation below $-\gamma$ is nearly parabolic. As we lower the chemical potential of the nanotube, we cross from the regime of the magnetic moment independent of R (conical dispersion relation near the Fermi points) to the regime where it depends linearly on R (quasi parabolic $E(\mathbf{k})$). The Brillouin zone in the intermediate regime is shown in Figs. 2 and 5b & c. The magnetic moment depends on the nanotube radius in a more complicated way (an example is shown in Fig. 4 as open circles). Note that its radius

dependence in the case of $E_F = \pm\gamma$ resembles that of persistent currents in metallic cylinders [16, 17].

Electron-hole symmetry of $\mu_{orb}(\phi, T)$. In temperatures up to 300K the $\mu_{orb}(\phi, T)$ for electron and hole doping are identical. This feature is found both when $\mu_{chem} = const$ and when $N_e = const$ (see Figs. 7–9, also Figs. 6 and 10). It is a combined effect of the symmetry of the Fermi-Dirac function with respect to the chemical potential, and the hole-electron symmetry of the dispersion relation of graphene which both enter Eq. (9) (for experimental confirmation see [18]).

Dependence of $\mu_{orb}(\phi, T)$ on the chirality of the nanotube. The shape of the Fermi contour in a CN changes significantly with doping [19], from two points (Fig. 5a), through a set of increasingly flattened circles (Fig. 5b,c), to a hexagone (Fig. 5d). That is why in doped nanotubes the form of the magnetic moment as a function of magnetic field and temperature depends strongly on the chirality of the nanotube and reflects the geometrical relation of their momentum lines to the actual shape of the Fermi surface. The paramagnetic contribution to the persistent current and consequently to the magnetic moment is enhanced if the number of states crossing simultaneously the Fermi level is large, therefore the strongest magnetic response should be achieved in systems with momentum lines nearly parallel to the Fermi surface [19]. This is achieved in a zigzag CN doped to $E_F = \pm\gamma$, where the lines of states (marked by black dots in Fig. 5d) are parallel to two sides of the Fermi surface (inner hexagone). The resulting magnetic moment is huge – see Fig. 9 and Tables I and II.

The shape of $\mu_{orb}(\phi, T)$ is different in isolated and connected nanotubes. This difference is illustrated in Figs. 7–9 for fields accessible in labs (up to 40T), and in Fig. 6 for the full ϕ_0 period.

Note for instance that in an isolated nanotube ($N_e = const$) the magnetic moment at half-filling (the line in the centre of the bottom row in Fig. 6) changes completely when even a few electrons are added or removed from the system. At constant chemical potential the dependence of $\mu_{orb}(\phi, T)$ on doping is more smooth.

Temperature dependence of $\mu_{orb}(\phi, T)$. The main effects of temperature on $\mu_{orb}(\phi, T)$ are a suppression of its amplitude and its smoothing into a sinusoidal shape. The former effect causes a decrease of the magnetic moment by a factor 2-3 over the temperature range from 0 to 300 K. Thus the measurements could be performed at room temperature which simplifies considerably the experiments.

The latter effect smoothes out all sharp features in the $\mu_{orb}(\phi, T)$ dependence and can even turn a diamagnetic moment at $T = 0$ into a paramagnetic one at $T = 300K$. This effect is seen for both isolated and connected nanotubes (see Fig. 7)

The sawtooth shape of the orbital magnetic moment in a $(38, 36) \times (-4028, 4101)$ nanotube doped to $\pm\gamma$ in Fig. 7 is a manifestation of the fractional period of the

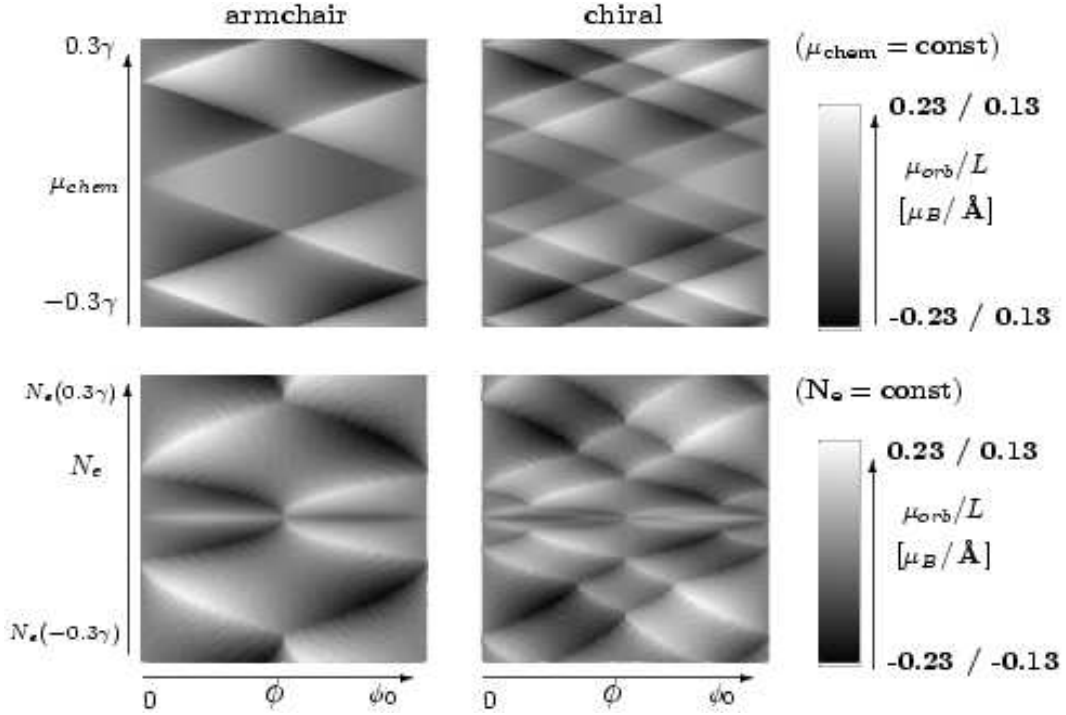


FIG. 6: The comparison between (top) $\mu_{chem} = const$ and (bottom) $N_e = const$ conditions on the conical part of the dispersion relation, i.e. for $|\mu_{chem}| \leq 0.3\gamma$. Left column shows the orbital magnetic moment per Å (colour scale) in armchair (15,15), right column - in chiral semiconducting (15,14) nanotubes.

Aharonov-Bohm effect, noticed by Sasaki et al. [20]. In CNs whose length is commensurate with their circumference, the period of the Aharonov-Bohm oscillations is a fraction of ϕ_0 .

The full dependence of $\mu_{orb}(\phi)$ on the doping, both in isolated ($N_e = const$) and connected ($\mu_{chem} = const$) nanotubes shows several interesting features. First, as long as the doping does not exceed $\pm 0.3\gamma$, the orbital magnetic moments fall in two distinct classes, depending on whether the nanotube was originally metallic or semiconducting. This feature appears in both conditions, in Fig. 10 we show it for $N_e = const$. It is due to the fact that the Fermi surface for small dopings is a set of nearly circular loops, meeting at the same angle the momentum lines of any chirality (cf. Fig. 5b).

As the Fermi surface loses the circular symmetry, at larger values of doping, differences appear between nanotubes of the same type of conduction and different chiralities (cf. Fig. 5c). This effect shows both in the case of nanotube isolated and forming part of a circuit. In Fig. 11 we show it for $\mu_{chem} = const$. The doping level at which the maximum amplitude of the magnetic moments is reached (marked by straight lines in Fig. 11) depends on the chirality of the CN.

V. CONCLUSIONS

CNs can be one of the basic ingredients of the future nanoelectronic devices. Therefore their behaviour in the magnetic field is of big importance. The magnetic field has a strong effect on the electronic structure of the CN – it can be used to tune the energy spectrum. This raises the possibility of controlling the energy levels through an external field, opening the door to further studies of fundamental properties of nanotubes as well as technological applications.

When applied parallel to the tube axis, the magnetic field creates orbital magnetic moments, which depend strongly on the chirality, length and doping level of the CN.

The results of our model calculations show that the behaviour of the orbital magnetic moment in single-wall nanotubes has the following features:

- 1) the temperature diminishes its amplitude and smoothes out sharp features in the $\mu_{orb}(\phi, T)$ dependence, which in doped nanotubes can even change the character of the response from diamagnetic at low T to paramagnetic at high T (cf. Fig. 7).
- 2) its dependence on ϕ is the same in electron- and hole-doped CNs in temperatures up to 300K, in nanotubes both isolated and forming part of a circuit
- 3) is nearly independent of R in half-filled CNs and depends on R in the doped ones

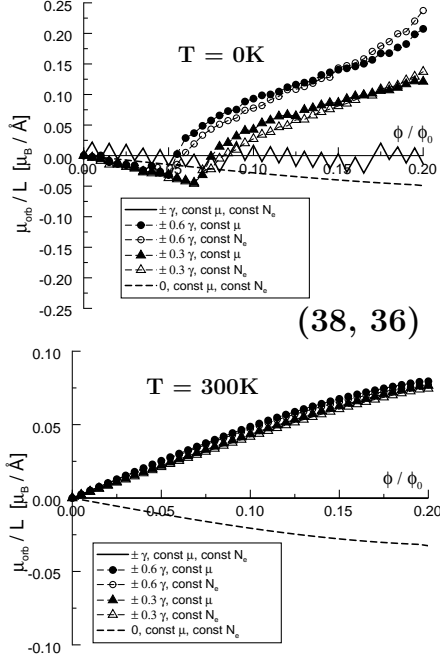


FIG. 7: The magnetic moment per unit length in a nearly armchair (38, 36) \times (−4028, 4101) nanotube, at $E_F = 0, \pm 0.3\gamma, \pm 0.6\gamma, \pm\gamma$, both for $\mu_{chem} = const$ and $N_e = const$, at $T = 0K$ and $T = 300K$. $R = 25\text{\AA}$, $\phi = 0.2\phi_0$ corresponds to $B = 40T$. The solid line, if not visible, coincides with the horizontal axis. At 300K the results for $\mu_{chem} = const$ and $N_e = const$ almost overlap.

- 4) scales with length in both pure and doped CNs
- 5) is independent of chirality for pure CNs and depends strongly on chirality in doped nanotubes.

It is well known that in the magnetic field parallel to the axis a metallic CN can be converted into a semiconducting one and vice versa [1]. This has been recently demonstrated as a change of the band gap in a series of experiments [2, 3, 4]. This extraordinary feature can be clearly seen also in the ϕ dependence of the orbital magnetic moment.

The nanotubes for which $\mu_{orb}(\phi, T)$ exhibits a steep rise are metallic, otherwise they are semiconducting. Inspection of e.g. Fig. 1 shows that the nanotube denoted by (m), metallic at $\phi \simeq 0$ transforms into a semiconducting one at $\phi \neq n\phi_0$ ($n \in \mathbb{Z}$), whereas the semiconducting nanotube denoted by (s) becomes metallic at $\phi = 1/3 \phi_0$ and $\phi = 2/3 \phi_0$. The maximum values of μ_{orb} in the range of 0-20 T are given in Tables I and II.

The relation between μ_{orb}^F calculated and measured in [2] and $\mu_{orb}(\phi, T)$ discussed in this paper is the following. μ_{orb}^F , being the magnetic moment of an electron at (or close to) the Fermi point, is calculated in the energy range where its dispersion relation is a linear function of \mathbf{k} , therefore μ_{orb}^F is independent of the flux. The total magnetic moment $\mu_{orb}(\phi, T)$ is calculated as a sum over

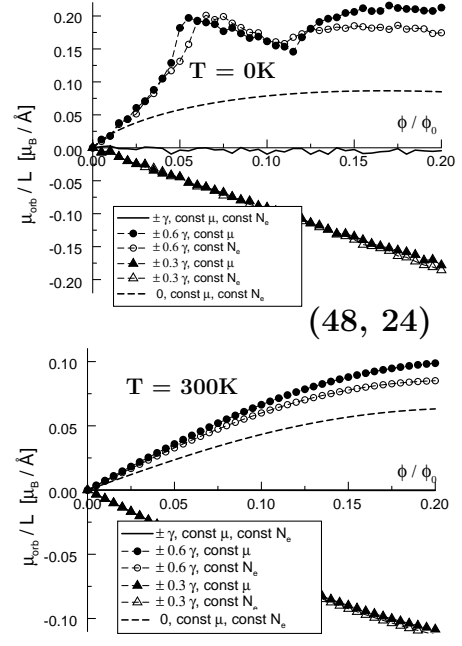


FIG. 8: The magnetic moment per unit length in a chiral metallic (48, 24) nanotube, at $E_F = 0, \pm 0.3\gamma, \pm 0.6\gamma, \pm\gamma$, both for $\mu_{chem} = const$ and $N_e = const$, at $T = 0K$ and $T = 300K$. $R = 25\text{\AA}$, $\phi = 0.2\phi_0$ corresponds to $B = 40T$. The solid line, if not visible, coincides with the horizontal axis.

all \mathbf{k} states, thus containing terms with nonlinear dispersion relation which cause the flux dependence of the magnetic moment. Moreover, $\mu_{orb}(\phi, T)$ calculated from Eq. (9) takes into account the temperature dependence of the energy level occupation. This effect has been neglected in the calculation of μ_{orb}^F .

Whereas the measurements of the band gap as a function of B give the information about μ_{orb}^F (which is actually the orbital moment unit, $\mu_{orb}^F = \pi R^2 I_0$, where $I_0 = \frac{e v_F}{2\pi R}$ is the unit of the persistent current), the full $\mu_{orb}(\phi, T)$ could be measured in other experiments which will be sensitive to it.

In our opinion this measurement may be possible in a setup with a double walled CN. The outer shell can be used as a field detector. The current running along it would be modified by the Aharonov-Bohm effect. The precise measurement of this current, compared with the current in identical but single-walled CN could reveal the magnetic moment produced by the inner tube.

In this paper we have given a survey of the properties of the orbital magnetic moments for single-wall nanotubes of different chiralities with different radii and length, and for various values of electron or hole doping, at zero and finite temperatures. In multiwall nanotubes these dependences are more complex, since all shells are penetrated by the magnetic field and all must be taken into account. The magnetic moments are then a superposition of moments from different shells. Some aspects of this problem

	$E_F = 0$	$E_F = \pm 0.3\gamma$	$E_F = \pm 0.6\gamma$	$E_F = \pm \gamma$
armchair (37,37)	78.7 (42.9)	-100 (-78.9)	-99.5 (-65.1)	≤ 3 (≤ 1)
chiral S (38,36)	-28.2(-20.5)	42.6 (43.5)	93.2 (48.6)	-26.4 (≤ 1)
chiral M (48,24)	78.7 (43.3)	-90.6 (63.9)	161.6 (66.4)	-9.7 (≤ 2)
chiral S (49,23)	-27.5 (-20)	218.8 (96.7)	-89.1 (-46.3)	≤ 2 (≤ 2)
chiral S (63,2)	-29.3(-21.8)	-116.9 (-72.7)	-148.1 (31.1)	399.2 (389)
zigzag M (63,0)	80.2 (44.1)	-62.5 (-28.7)	28.7 (-63.1)	-714.7 (-523)
zigzag S (64,0)	-29.8 (-21.9)	-113.3 (-73.2)	-290 (21.8)	3559 , at $B \ll 1\text{T}$ (818.2)

TABLE I: Magnetic orbital moment at $\mu_{\text{chem}} = \text{const}$ for SWNT of radius 25\AA , length $0.1\mu\text{m}$, for various chiralities and levels of electron or hole doping E_F . The unit is μ_B , values in brackets (italics) are for $T = 300\text{K}$, outside brackets for $T = 0\text{K}$. The orbital moments greater than $100\mu_B$ are in bold font. The values in the table are the maximum values obtainable in magnetic fields ranging from 0 to 20T. Typically this maximum value is reached at 20T, except for one case, (64,0) doped to $\pm\gamma$.

	$E_F = 0$	$E_F = \pm 0.3\gamma$	$E_F = \pm 0.6\gamma$	$E_F = \pm \gamma$
armchair (37,37)	78.7	-107	-105.5	4.44
chiral S (38,36)	-28.2	-41.9 ($B \simeq 12\text{T}$)	77.7	19.6 ($B \simeq 18\text{T}$)
chiral M (48,24)	78.7	-92.7	194.5 ($B \simeq 14\text{T}$)	-9.65
chiral S (49,23)	-27.5	225	-94.8	-3.48
chiral S (63,2)	-29.3	-115.4	-223.8	395.9
zigzag M (63,0)	80.2	-69.5	-11.9	-714.7
zigzag S (64,0)	-29.8		-293	3559 , at $B \ll 1\text{T}$

TABLE II: Magnetic orbital moment at $\mathbf{N}_e = \text{const}$ for SWNT of radius 25\AA , length $0.1\mu\text{m}$, for various chiralities and levels of electron or hole doping. The unit is μ_B , $T = 0\text{K}$. The orbital moments greater than $100\mu_B$ are in bold font. The values in the table are the maximum values obtainable in magnetic fields ranging from 0 to 20T. Typically this maximum value is reached at 20T, if otherwise, the corresponding approximate value of B is indicated.

have recently been discussed in [13, 21].

(solicited) grant No PBZ-MIN-008/P03/2003.

M.S. thanks H  l  ne Bouchiat for valuable discussions.

Acknowledgments

This work was supported by the Polish Ministry of Scientific Research and Information Technology under the

-
- | | |
|---|--|
| <p>[1] H.Ajiki, T.Ando, <i>J. Phys. Soc. Japan</i> 62 (1993) 2470</p> <p>[2] E.D. Minot, Y. Yaish, V. Sazonova, P. McEuen, <i>Nature</i> 428 (2004) 536</p> <p>[3] U.C. Coskun, T.-C. Wei, S. Vishveshwara, P.M. Goldbart, A. Bezryadin, <i>Science</i> 304 (2004) 1132</p> <p>[4] S. Zaric, G.N. Ostojic, J. Kono, J. Shaver, V.C. Moore, M.S. Strano, R.H. Hauge, R.E. Smalley, X. Wei, <i>Science</i> 304 (2004) 1129</p> <p>[5] M.B  ttiker, Y. Imry, R. Landauer <i>Phys. Lett A</i> 96 (1983) 365</p> <p>[6] H.-F. Cheung, Y. Gefen, E.K. Riedel, W.-H. Shih, <i>Phys. Rev. B</i> 37 (1988) 6050</p> <p>[7] B. Reulet, M. Ramin, H. Bouchiat, D. Mailly, <i>Phys. Rev. Lett.</i> 75 (1995) 124</p> <p>[8] T.W. Odom, J.-L. Huang, P. Kim, C.M. Lieber, <i>J. Phys. Chem B</i> 104 (2000) 2974</p> | <p>[9] S. Latil, S. Roche, A. Rubio, <i>Phys. Rev B</i> 67 (2003) 165420</p> <p>[10] J. Gonzalez, F. Guinea, M.A.H. Vozmediano, <i>Int J. Mod Phys B</i> 112 (1993) 4331</p> <p>[11] R. Saito, G. Dresselhaus, M.S. Dresselhaus <i>Physical Properties of Carbon Nanotubes</i>, Imperial College Press, London 1998</p> <p>[12] F. Bloch, H. Rorschach <i>Phys. Rev.</i> 128 (1962) 1697</p> <p>[13] M. Marga  ska, M. Szopa, E. Zipper, <i>Acta Phys. Pol. A</i> 106 (2004) 609</p> <p>[14] M.F. Lin, D.S. Chuu, <i>Phys. Rev. B</i> 57 (1998) 6731</p> <p>[15] P.L. McEuen, M. Bockrath, D.H. Cobden, Y.-G. Yoon, S.G. Louie, <i>Phys. Rev. Lett.</i> 83 (1999) 5098</p> <p>[16] H. Cheung, Y. Gefen, E.K. Riedel, <i>IBM J. Res. Develop.</i></p> |
|---|--|

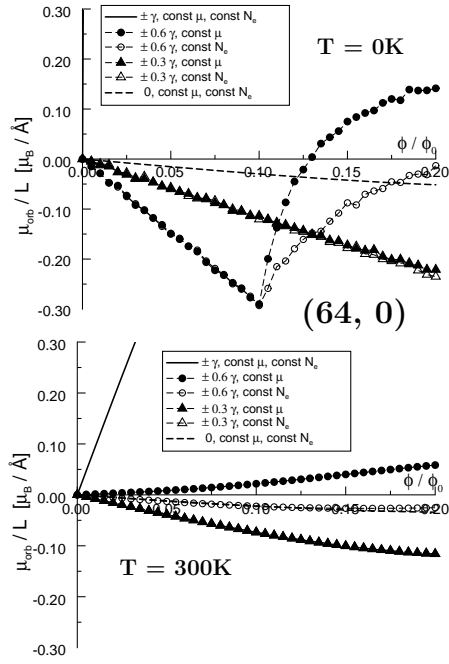


FIG. 9: The magnetic moment per unit length in a zigzag (64,0) nanotube, at $E_F = 0, \pm 0.3\gamma, \pm 0.6\gamma, \pm\gamma$, both for $\mu_{chem} = const$ and $N_e = const$, at $T = 0K$ and $T = 300K$. $R = 25\text{\AA}$, $\phi = 0.2\phi_0$ corresponds to $B = 40T$. The magnetic moment at $\mu_{chem} = \pm\gamma$ and $T = 0K$ in the zigzag nanotube is a very steep function of ϕ (see [19]) and overlaps with the vertical axis on this plot. At 300K the results for $\mu_{chem} = const$ and $N_e = const$ overlap.

- 32** (1988) 359
- [17] M. Stebelski, M. Szopa, E. Zipper, *Z.Phys B* **103** (1997) 79
 - [18] P. Jarillo-Herrero, S. Sapmaz, C. Dekker, L.P. Kouwenhoven, H.S.J. van der Zant, *Nature* **429** (2004) 389
 - [19] M. Szopa, M. Margańska, E. Zipper, *Phys. Lett. A* **299** (2002) 593
 - [20] K. Sasaki, S. Murakami, R. Saito, *Phys. Rev. B* **70** (2004) 233406
 - [21] M. Szopa, M. Margańska, E. Zipper, M. Lisowski, *Phys. Rev. B* **70** (2004) 075406

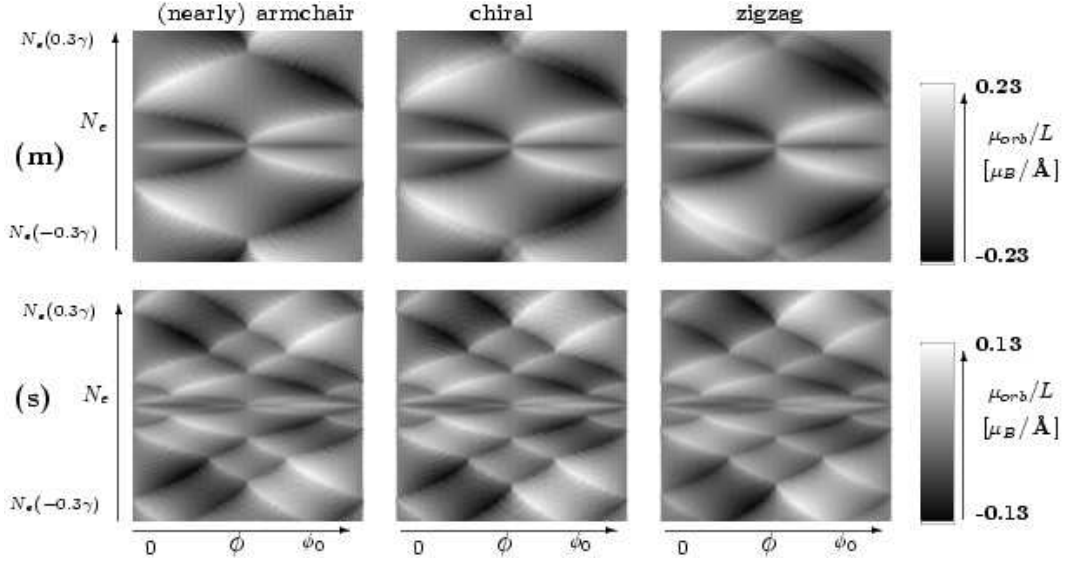


FIG. 10: The orbital magnetic moment per Å (colour scale) for $|\mu_{chem}| \leq 0.3\gamma$, for metallic (top row) armchair (15,15), chiral (19,10), zigzag (24,0) nanotubes, and for semiconducting (bottom row) nanotubes with similar chiralities – (15,14), (19,9) and (25,0). $R = 10.2\text{\AA}$, $T = 0$. The Fermi contour around a Fermi point in this regime is almost circular, which accounts for the similarities between the three cases.

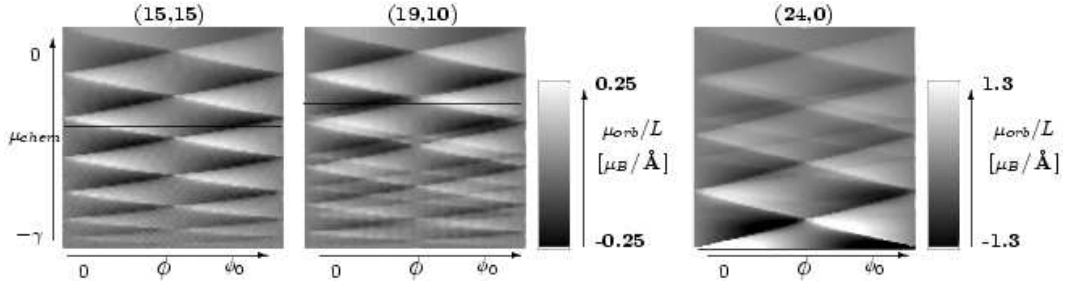


FIG. 11: The magnetic moment per Å (colour scale) in (15,15) armchair (left), (19,10) chiral metallic (middle) and (24,0) metallic zigzag (right) hole-doped nanotubes ($R = 10.2\text{\AA}$). The range of chemical potential is from $-\gamma$ to 0. The part corresponding to electron-doped nanotube is symmetrical to the hole-doped. At the chemical potential lower than $\sim -0.3\gamma$ (lower part of the plots), the Fermi contour ceases to be circular and the μ_{orb} patterns become different for different chiralities. The maximum amplitude of the magnetic moment is in each nanotube reached at a different value of doping, marked by a straight line.